Proceedings of the Seventh International Conference on
Railway Technology: Research, Development and Maintenance
Edited by: J. Pombo
Civil-Comp Conferences, Volume 15, Paper 5.7
Civil-Comp Press, Edinburgh, United Kingdom, 2026
ISSN: 2753-3239, doi: 10.4203/ccc.15.5.7
©Civil-Comp Ltd, Edinburgh, UK, 2026

Study on Drag Reduction by Air Blowing and Suction for High-speed Maglev Trains

G. Li[1,2], J. Du[3,2], S. Fu[3,2], D. Chen[3,2], S. Ding[3,2], J. T. Du[3,2] and N. Liu[3]

[1]CRRC Qingdao Sifang Co. Ltd, China
[2]State Key Laboratory of High-speed Maglev Transportation Technology, China
[3]CRRC Qingdao Sifang Co., Ltd., China

Abstract

High-speed maglev trains, as an important component of future urban transportation systems, have drawn continuous attention regarding their operational efficiency and energy utilization. This study aims to explore the use of air blowing and suction technology to reduce air resistance during maglev train operation, thereby improving operational efficiency and reducing energy consumption. Using computational fluid dynamics (CFD) methods, the research investigates the evolution characteristics of the boundary layer on the surface of high-speed maglev trains and the distribution of aerodynamic resistance. By setting blowing and suction holes in the transition area between the streamlined head and the uniform cross-section body of the train, a blowing and suction boundary layer control scheme is proposed to reduce resistance. Through numerical simulations of the aerodynamic drag of the train with blowing and suction holes set in three different regions: before the separation point, including the separation point, and after the separation point, the impact of the blowing and suction techniques on train drag is analyzed. In the suction mode, when the suction speed reaches a certain value, the aerodynamic resistance of the vehicle decreases; in the blowing mode, the aerodynamic resistance of the vehicle increases at most blowing speeds; Within the studied suction speed range, the drag reduction rate increases with increasing suction speed, with the maximum drag reduction rate of the entire train reaching 3.26%. The results provide new insights for aerodynamic drag reduction of high-speed maglev trains.

Keywords: high-speed maglev train, boundary layer, aerodynamic drag reduction, blowing and suction, computational fluid dynamics, flow control.

1 Introduction

With the development of computational technology and optimization theories, a large number of researchers have been devoted to the study of aerodynamic shape optimization of rail vehicles to achieve drag reduction, resulting in a series of substantial research outcomes [1-5]. Aerodynamic shape optimization alters the external flow field structure of the vehicle by changing the shape of the vehicle head or guiding the flow around areas such as the bogie and pantograph, thereby reducing the aerodynamic drag of the train. Traditional aerodynamic shape optimization has become increasingly refined and mature, but it is also showing limitations due to the continuous improvement in manufacturing processes and design requirements. Applying new theories and technologies for train aerodynamic drag reduction design has become an inevitable trend.

In recent years, blowing and suction flow control techniques have increasingly become a research hotspot in the field of rail vehicle aerodynamics. Gao et al. [6], using numerical methods, explored the effects of jet flow at different positions and speeds on the turbulent flow field and aerodynamic drag around high-speed trains. They proposed a blowing drag reduction scheme at the tail of the train, achieving a maximum drag reduction rate of 3.84%. Lin et al. [7] used simulation methods to study the evolution characteristics of the boundary layer on the surface of high-speed trains and the distribution law of aerodynamic drag by setting suction holes in the flow separation zones at the boundary layer separation points of the train's head and tail cars. The results showed that setting suction holes in the flow separation zones of the head and tail cars reduced the aerodynamic drag coefficient of the whole train, with a maximum drag reduction rate of 6%. Liang et al. [8] studied the drag reduction technology of low-density gas injection on the surface of high-speed trains. They found that injecting low-density gas significantly reduces the density of the gas medium in the boundary layer, resulting in better drag reduction. However, as the gas density increases, the pressure drag between the front and rear of the jet increases, thereby increasing the train's drag. Cui et al. [9] proposed an active flow control drag reduction method combining suction and blowing at the tail of EMU trains. Based on a three-car EMU, they analyzed the effects of different mass flow rates, positions, and numbers of suction and blowing holes on the aerodynamic drag and surface pressure of the EMU tail. The results indicated that tail suction and blowing could reduce the pressure drag of EMUs. Chen et al. [10] studied the drag reduction effect of blowing at the head and tail cars of high-speed trains. The blowing measures create an air gap between the incoming flow and the train surface, thereby reducing viscous and pressure drag. At optimal blowing speeds, the overall aerodynamic drag coefficient of the train decreased by 10.78%. Jin et al. [11] studied the effect of setting blowing interfaces in the streamlined regions at the front and rear of the train to alleviate tunnel pressure waves. The results showed that the overall amplitude effect of the pressure waves was independent of the position of the blowing interface, and when the blowing speed reached 20 m/s, the minimum pressure value at the train body decreased by 33% to 56%, and the maximum pressure value at the tunnel entrance decreased by about 28%.

In the field of high-speed maglev trains, Che et al. [12] explored the effects of blowing on aerodynamic drag and wake characteristics, studying the drag reduction effect and wake field characteristics of adding blowing slots on the surface of the TR08 maglev train's tail car and blowing in three different directions at two different speeds. The results showed that blowing only in the flow direction at a speed of 24 m/s resulted in a drag reduction effect of up to 6.53%. Moreover, blowing significantly reduced the aerodynamic lift of the tail car, providing new insights into the stability control of maglev vehicles. Chen et al. [13] proposed a suction technique to suppress pressure waves by setting suction slots on the tunnel walls. After activating the suction slots, a low-pressure zone is created near the suction slots, which can weaken the initial compression wave and the high-pressure zone in front of the train, thereby mitigating the pressure waves generated when high-speed maglev trains pass through tunnels and significantly improving the tunnel's aerodynamic conditions. Guo et al. [14] evaluated the effectiveness of windward side blowing methods in reducing the lateral aerodynamic impact of high-speed maglev trains at different yaw angles. The study results showed that active blowing mixed with the transverse downstream airflow on the train roof increased local turbulence and changed the surface pressure distribution. Within the studied yaw angle range, active blowing reduced the lateral force by 1.0% to 8.8%. Overall, these studies highlight the diverse applications and effectiveness of blowing and suction technologies in advancing high-speed maglev train technology, contributing to their aerodynamic optimization and operational efficiency.

This paper proposes a drag reduction scheme by setting blowing and suction holes in the flow separation zones at the boundary layer separation points of the train's head cars. By performing numerical simulations on the aerodynamic drag of the train under different blowing and suction parameters, the study investigates the influence of the blowing and suction technology on train drag, providing a reference for aerodynamic drag reduction in high-speed maglev trains.

2 Methods

The simulation calculations were performed using a three-carriage maglev train model. The computational domain and boundary conditions are shown in Figure 1. The height of the train, H, is used as the characteristic length, with the train and track beam located in the middle of the computational domain. The leading car is 30H away from the inlet boundary, and the trailing car is 60H away from the outlet boundary to ensure the formation and shedding of the trailing vortices. The height and width of the computational domain are 15H and 30H, respectively. The inlet, outlet, top surface, and two sides of the computational domain are all set as free-stream boundary conditions. The ground and track beam are set as slip ground boundary conditions, with speeds consistent with the train's running speed, while the train body surface is given no-slip surface boundary conditions.

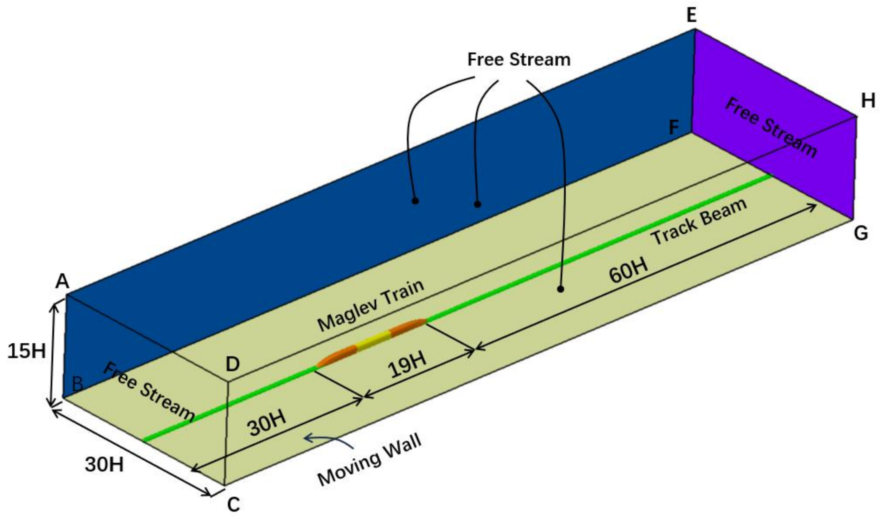

Figure 1: Computational domain and boundary conditions.

The high-speed maglev train can reach speeds of up to 600 km/h, which is 0.5 Mach and greater than 0.3 Mach. At this point, the fluid in the flow field is considered compressible flow, and the compressible Navier-Stokes (NS) equations are used as the numerical solution governing equations. The finite volume method is applied to convert the governing equations into a discrete form that can be solved numerically. A second-order upwind scheme is used for the convective terms, a second-order central scheme for the viscous terms, and the k-ω SST model is adopted for the turbulence model.

The StarCCM+ software is used to establish a hexahedral grid. The spatial grid type is Trimmer grid, with boundary layer grids arranged on the train body surface. The height of the first layer is 0.8 mm with a growth ratio of 1.2, and a total of 6 layers of boundary layer grids. To better simulate the flow field structure around the vehicle, local refinement is carried out on the vehicle wall surface and wake region, with a total grid quantity of about 40 million.

3 Results

Since the boundary layer separates at the transition position between the streamlined head car and the constant cross-section car body of the high-speed maglev train, blowing and suction holes are set near this area. As shown in Figure 2, 10 rows of blowing and suction holes are arranged near the flow separation point of the high-speed maglev train's leading car, and these are divided into three regions: Area 1: the area before the separation point (rows 1-4); Area 2: the area containing the separation point (rows 4-7); Area 3: the area after the separation point (rows 7-10). The hole diameter is chosen as D=80 mm, and the hole spacing is 3R.

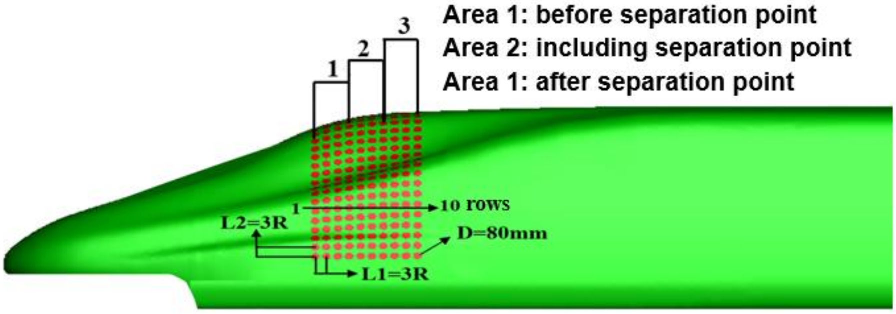

Figure 2: Setting of air blowing and suction holes.

Blowing and suction speeds of 0.1U to 1.0U are selected, with ten speed levels (where U represents the train speed of 250 km/h). Numerical calculations of the aerodynamic drag coefficient of the entire high-speed maglev train are performed for blowing and suction at different region positions. This paper introduces the relative value of the aerodynamic drag coefficient C_{ref} to express the changes in aerodynamic drag under different blowing and suction speeds, calculated as:

$$C_{ref} = C_d/C_{d\text{-}former} \tag{1}$$

where C_d and $C_{d\text{-}former}$ are the aerodynamic drag coefficients with and without blowing and suction, respectively. To facilitate the evaluation of the drag reduction effect of the train, the drag reduction rate x% is introduced, defined as:

$$x\% = (1-C_{ref})\times 100\% \tag{2}$$

3.1 Suction Control

Figure 3 shows the drag reduction rates of the train's aerodynamic drag with suction control at different speeds in three regions: Area 1 (before the separation point), Area 2 (including the separation point), and Area 3 (after the separation point) for the streamlined leading car of the high-speed maglev train.

From Figure 3, it can be observed that when suction control is applied in the three regions, the drag reduction rate of the train's aerodynamic drag is negative (indicating increased drag) when the suction speed is less than 0.4U in any region. As the suction position moves from Area 1 to Area 3, the increase in drag rate gradually decreases. When the suction speed reaches 0.4U, a drag reduction effect begins to appear in Areas 2 and 3, while suction in Area 1 still results in increased drag. When the suction speed exceeds 0.4U, suction in any region has a drag reduction effect, with the best drag reduction effect in Area 2.

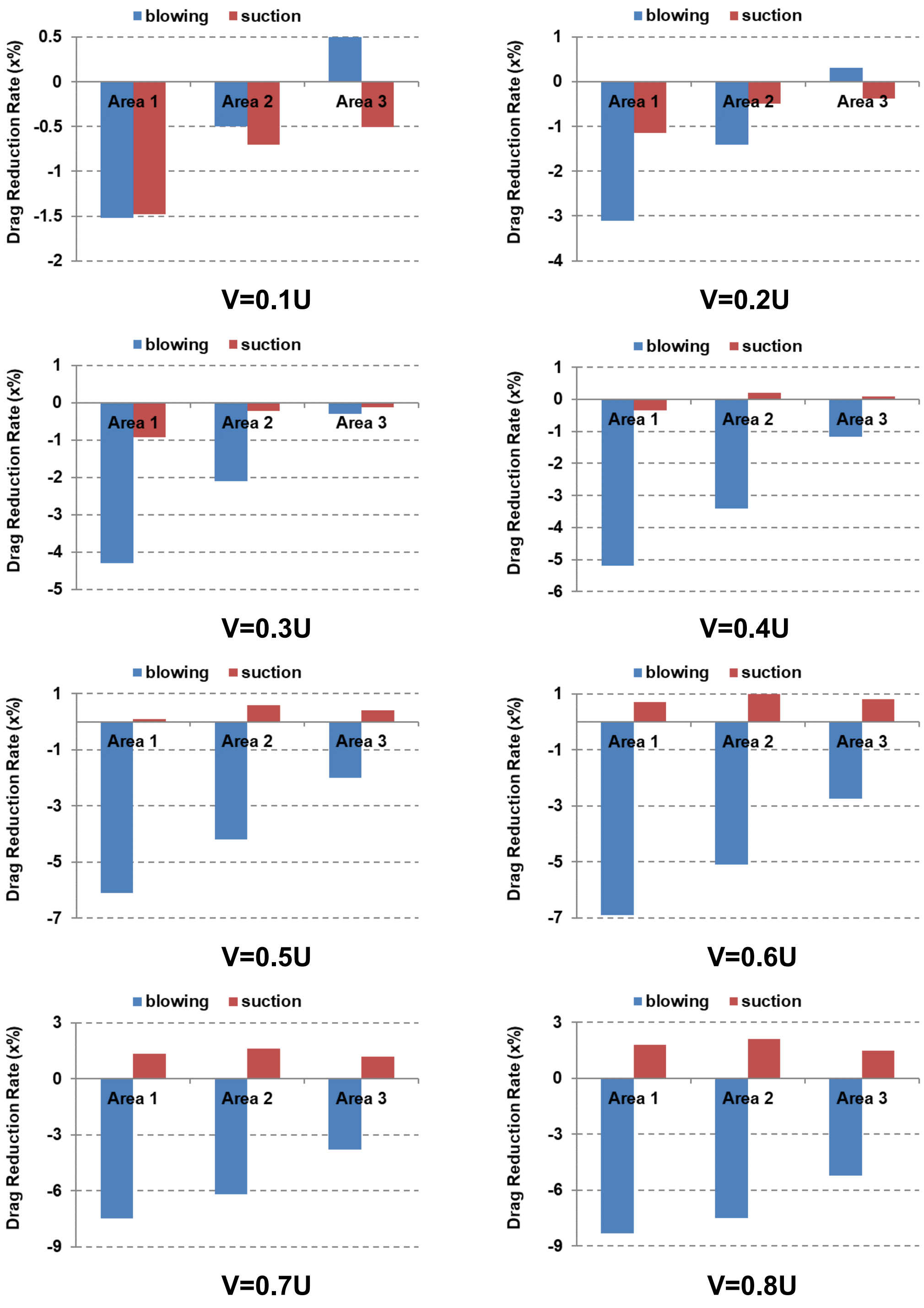
blowing
suction
Drag Reduction Rate (x%)
Area 1
Area 2
Area 3
V=0.1U
V=0.2U
V=0.3U
V=0.4U
V=0.5U
V=0.6U
V=0.7U
V=0.8U

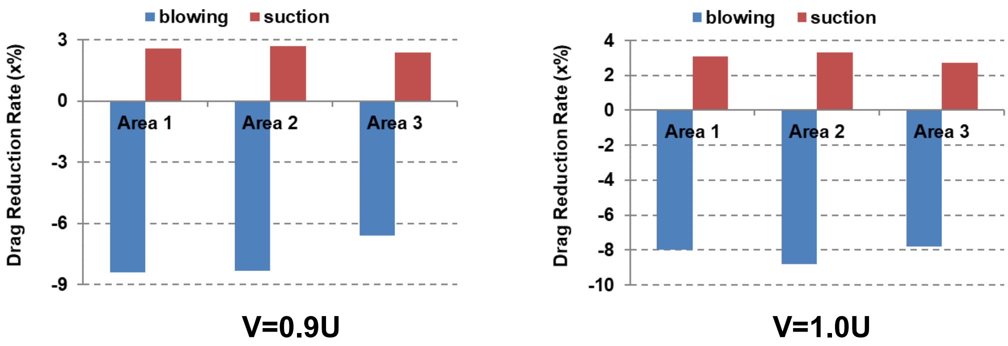

Figure 3: Changes in vehicle drag reduction rate when blowing and inhaling air at different speeds in different areas.

The aerodynamic drag of high-speed maglev trains is mainly composed of pressure drag and friction drag. Decomposing the proportion of these two types of drag in the drag reduction by blowing and suction control on the train surface is crucial for further research and improvement of drag reduction methods. This paper provides a detailed analysis of the pressure drag and friction drag of the entire vehicle during suction in different regions. The suction speeds are taken as the characteristic values in the above three regions: 0.1U (no drag reduction effect), 0.4U (beginning to have a drag reduction effect), and 1.0U (drag reduction effect in all regions). Table 1 presents the relative values of pressure drag, friction drag, and total drag coefficients of the train under suction at different speeds in different regions. In the table, D_p represents pressure drag, D_f represents friction drag, and D_t represents total drag. The trends of the drag reduction rates of pressure drag, friction drag, and total drag with suction speed are shown in Figure 4.

In Figure 4(a), the pressure drag reduction rate gradually increases with the increase in suction speed. Areas 2 and 3 achieve a drag reduction effect when the suction speed is greater than 0.25U, while the suction speed in Area 1 needs to be greater than 0.35U to achieve a drag reduction effect. In Figure 4(b), the friction drag reduction rate rapidly decreases to a negative value with the increase in suction speed, indicating increased drag. From the total drag in Figure 4(c), it can be seen that only when the suction speed is greater than 0.4U does the contribution of pressure drag to drag reduction surpass that of friction drag, resulting in a drag reduction effect on the total drag.

Table 1: Relative values of train pressure difference and friction resistance coefficient when air is sucked at different speeds in different areas.

Cref	V=0.1U			V=0.4U			V=1.0U		
	D_p	D_f	D_t	D_p	D_f	D_t	D_p	D_f	D_t
Area 1	1.0252	0.9962	1.0147	0.9941	1.0211	1.0039	0.9256	1.0435	0.9683
Area 2	1.0126	0.9981	1.0073	0.9841	1.0233	0.9983	0.9247	1.0423	0.9674
Area 3	1.0085	0.9996	1.0053	0.9847	1.0239	0.9989	0.9384	1.0296	0.9715

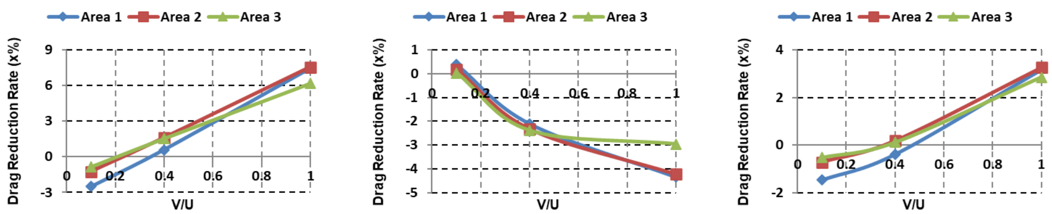

(a) pressure drag (b) friction drag (c) total drag

Figure 4: Aerodynamic drag reduction rate changes with speed during suction.

3.2 Blowing Control

From Figure 3, it can also be seen that when blowing control is used, only Area 3 (after the separation point) shows a slight drag reduction effect at blowing speeds of 0.1U and 0.2U, with a maximum drag reduction rate of only 0.46%. Blowing at different speeds in other regions increases the train's aerodynamic drag.

A detailed analysis of the changes in drag reduction rates of pressure drag, friction drag, and total drag at blowing speeds of 0.1U, 0.2U, and 0.5U in the three regions is performed. Table 2 presents the relative values of pressure drag, friction drag, and total drag coefficients of the train under blowing at speeds of 0.1U, 0.2U, and 0.5U in different regions. The trends of the drag reduction rates of pressure drag, friction drag, and total drag with blowing speed are shown in Figure 5.

From Figure 5, it can be seen that blowing at the transition position between the streamlined head and the constant cross-section car body of the leading car results in a negative pressure drag reduction rate, indicating increased drag, while the friction drag reduction rate is positive, indicating reduced drag. When the blowing speed is relatively low (less than 0.2U), the friction drag reduction rates in the three regions do not differ much, but the pressure drag increase rate gradually decreases as the blowing position moves backward. Thus, blowing in Area 3 has a slight drag reduction effect. However, in Areas 1 and 2, the increase in pressure drag is greater than the reduction in friction drag, resulting in an overall increase in total drag. When the blowing speed exceeds 0.2U, the pressure drag increase rates in all regions rapidly increase, with the increase rate greater than the reduction rate of friction drag, leading to an overall increase in total aerodynamic drag of the entire train.

Table 2: Relative values of train pressure difference and friction coefficient when blowing air at different speeds in different areas.

Cref	V=0.1U			V=0.2U			V=0.5U		
	D_p	D_f	D_t	D_p	D_f	D_t	D_p	D_f	D_t
Area 1	1.0562	0.9437	1.0154	1.0918	0.9244	1.0311	1.1504	0.8987	1.0591
Area 2	1.0394	0.9450	1.0051	1.0657	0.9247	1.0146	1.1229	0.9002	1.0421
Area 3	1.0227	0.9466	0.9951	1.0381	0.9250	0.9971	1.0871	0.9025	1.0201

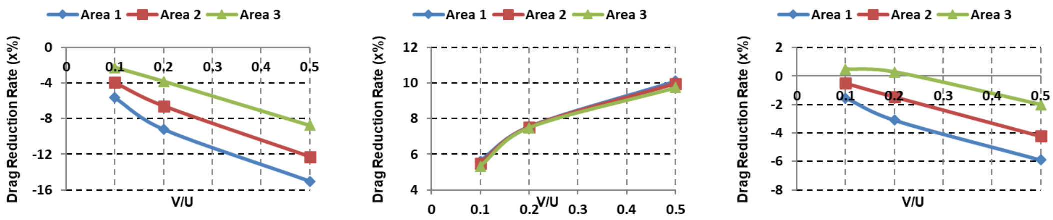

(a) pressure drag (b) friction drag (c) total drag

Figure 5: Aerodynamic drag reduction rate changes with speed during blowing.

4 Conclusions and Contributions

Using numerical simulations, the drag reduction effects of blowing and suction boundary layer control in the flow separation area of the leading car of a high-speed maglev train were studied. The following conclusions were obtained:

(1) When applying suction control in three different regions (before the separation point, including the separation point, and after the separation point), if the suction speed is less than 0.4U, the aerodynamic drag reduction rate of the train is negative in any region, indicating increased drag. At a suction speed of 0.4U, drag reduction effects begin to appear in Areas 2 and 3, while Area 1 still shows increased drag. When the suction speed exceeds 0.4U, suction in any region results in a drag reduction effect, with Area 2 showing the best drag reduction effect.

(2) The overall drag reduction rate increases with the increase in suction speed. In Area 2, the overall drag reduction rate can reach up to 3.26% when the suction speed is 1.0U.

(3) When applying blowing control in the three regions, only Area 3 (after the separation point) shows a certain drag reduction effect at blowing speeds of 0.1U and 0.2U. Blowing at different speeds in other regions increases the aerodynamic drag of the train.

References

[1] Shuanbao Yao, Dilong Guo, Guowei Yang, et.al. "Distribution of High-speed Train Aerodynamic Drag", Journal of the China Railway Society, 2012.

[2] Jiali Liu, Aiqin Tian, Jian Du, et.al. “Influence of head control line shape on aerodynamic noise of high-speed train”, Chinese Railways, 2014.
[3] Zhixiang Huang, Li Chen, Keling Jiang. “Wind Tunnel Test of Air-drag Reduction Schemes of High-speed Trains”, Journal of the China Railway Society, 2012.
[4] Guibo Li, Jian Du, Aiqin Tian, et.al. “Aerodynamic Optimization of the Head Shape of a High-speed Train Based on Adjoint Method”, Proceedings of the 2nd International Conference on Industrial Aerodynamics, Qingdao, China, DEStech Publications, Inc. 2017.
[5] Gecheng ZHA, Wei GAO, D. PAXTON, CRAIG. “Jet Effects of Coflow Jet Airfoil Performance”, AIAA Journal, 2007.
[6] Na Gao, Jian Du. “Research on Drag Reduction Flow Control Technology for High-Speed EMUs”, 2022 International Conference on Mechanics and Applied Mathematics, 2022.
[7] Peng Lin, Guibo Li. “Numerical study on the aerodynamic drag reduction characteristics of high speed train suction based on the drag reduction theory of boundary layer”, China Railway, 2020.
[8] Xifeng Liang, Zhangjun Luo, Xiaobai Li, Xiaohui Xiong, Xin Zhang. “Drag reduction of high-speed trains via low-density gas injection”, AIP Advances, 2022.
[9] H Cui, G Chen, Y Guan, W Deng, “Study on aerodynamic drag reduction at tail of 400 km/h EMU with air suction-blowing combination”, Machines, 2023.
[10] ZW Chen, GZ Zeng, YQ Ni, TH Liu, JQ Niu, “Reducing the aerodynamic drag of high-speed trains by air blowing from the nose part: Effect of blowing speed”, Journal of Wind Engineering and Industrial Aerodynamics, 2023.
[11] K Jin, L Zhang, X Li, L Li, J Chen, J Wang, “Effect of characteristic parameters of air-bleeding/blowing interface on tunnel pressure waves in streamlined regions of high-speed trains: A numerical simulation”, Sustainable Cities and Society, 2024.
[12] ZX Che, ZW Chen, YQ Ni, S Huang, ZW Li, “Research on the impact of air-blowing on aerodynamic drag reduction and wake characteristics of a high-speed maglev train”, Physics of Fluids, 2023.
[13] ZW Chen, ZH Guo, YQ Ni, TH Liu, J Zhang, “A suction method to mitigate pressure waves induced by high-speed maglev trains passing through tunnels”, Sustainable Cities and Society, 2023.
[14] ZJ Guo, ZW Chen, ZX Che, A Bordbar, YQ Ni, “Using leeward air-blowing to alleviate the aerodynamic lateral impact of trains at diverse yaw angles”, Physics of Fluids, 2024.